Transferrable monolithic multicomponent system toward near-ultraviolet optoelectronics

Chuan Qin[1], Xumin Gao[1], Jialei Yuan[1], Zheng Shi[1], Yuan Jiang[1], Yuhuai Liu[2,*], Yongjin Wang[1,*], and Hiroshi Amano[3,*]

[1]*Peter Grünberg Research Centre, Nanjing University of Posts and Telecommunications, Nanjing 210003, China*

[2]*Department of Electronics Engineering, Zhengzhou University, Science Road 100, Zhengzhou 450001, China*

[3]*Institute of Materials and Systems for Sustainability, Nagoya University, Nagoya 464-8062, Japan*

* Correspondence to: ieyhliu@zzu.edu.cn; wangyj@njupt.edu.cn; amano@nuee.nagoya-u.ac.jp

***Abstract**:* A monolithic near-ultraviolet multicomponent system is implemented on a 0.8-mm-diameter suspended membrane by integrating a transmitter, waveguide, and receiver into a single chip. Two identical InGaN/$Al_{0.10}Ga_{0.90}N$ multiple-quantum-well (MQW) diodes are produced by using the same process flow, which separately function as a transmitter and receiver. There is a spectral overlap between the emission and detection spectra of the MQW diodes. Therefore, the receiver can respond to changes in the emission of the transmitter. The multicomponent system is mechanically transferred from silicon, and the wire-bonded transmitter on glass experimentally demonstrates spatial light transmission at 200 Mbps using non-return-to-zero on-off keying modulation.

III-nitride ultraviolet multiple-quantum-well (MQW) diodes are often investigated as light-emitting diodes (LEDs), which have become an emerging topic for a variety of potential applications from water purification to biological detection, medical diagnostics, sterilization, and environmental sensing [1-5]. In fact, an MQW diode that integrates the MQW bandgap structure to generate light emission corresponding to the energy gap can also function as a photodiode to sense light [6]. The light emission of the MQW diode exhibits a broad spectrum, and an overlap exists between the emission and detection spectra of the MQW diode. Consequently, the high-energy photons can be detected by the MQW-diode itself. The simultaneous light-emitting, light-detecting behavior of the MQW-diode enables the monolithic III-nitride photonic integration of a transmitter, waveguide, modulator, and receiver within a single chip. On the basis of the dual functioning of InGaN/GaN MQW-diodes, significant attention has been devoted to exploring monolithic III-nitride multicomponent systems with integrated functionalities. Employing with the self-interference cancellation technique, a III-nitride integrated photonic circuit has demonstrated full-duplex in-plane visible-light communication [7]. Without changing the MQW structure, decreasing the electrode-size will increase the modulation rate but decrease the light emission intensity of the MQW-diode. Device optimization will be required for high-speed monolithic multicomponent system based on III-nitride micro- and nano-LEDs [8, 9]. Monolithic InGaN photonic integration has been developed for multifunctional devices [10, 11]. Sharing an identical MQW structure, multiple optical components with different functions are produced with a compatible process flow and merged together, providing great potential for optical interconnect applications.

On the other hand, with the advances in the growth of high-quality III-nitride films on silicon substrates [12-15], III-nitride optoelectronics on silicon are of great interest to researchers

[5]. Since the MQW structure creates light with the wavelength of the smaller-bandgap material, the generated light can be tuned by adjusting the bandgap material [16, 17]. Li *et al.* adopted an AlN/AlGaN buffer layer with a step-graded Al composition to grow a thick $Al_{0.05}Ga_{0.95}N$ layer for stress compensation, leading to the formation of low-In-content InGaN/$Al_{0.10}Ga_{0.90}N$ LEDs on a Si (111) substrate [18]. Zhang *et al*. deposited an AlGaN/Al buffer layer before growing a crack-free thick GaN layer, and demonstrated ~370 nm $In_{0.03}Ga_{0.97}N/Al_xGa_{1-x}N$ LEDs on Si (001) substrates [19]. In comparison with a sapphire substrate, the III-nitride-on-silicon platform offers advantages for mass production. Suspended waveguide architectures with a large index difference between air and III-nitride materials can be readily obtained by a combining well-developed silicon removal and backside III-nitride thinning techniques.

Here, we propose the fabrication and characterization of a transferrable monolithic near-ultraviolet (NUV) multicomponent system with multiple functionalities on III-nitride-on-silicon platform. Two identical InGaN/$Al_{0.10}Ga_{0.90}N$ MQW-diodes are produced using the same fabrication process flow and separately a transmitter and receiver, respectively. The multicomponent system integrates a transmitter, waveguide and receiver into a 0.8-mm-diameter suspended membrane, which is mechanically released by fracturing the support beams [20-22]. The transferred monolithic multicomponent system on glass exhibits integrated functionalities for versatile applications [23-25]. It is essential to future optoelectronic systems, which will be built up on a flexible substrate with diverse functionalities by multiple crucial devices.

Figure 1(a) shows a cross-sectional transmission electron microscopy (TEM) image of III-nitride films on a Si (111) substrate. Between the silicon and the thick AlGaN layer, there are large mismatches in both the lattice constant and the coefficient of thermal expansion. To overcome the problem, an AlN/AlGaN multilayer buffer with a step graded Al composition is

deposited on the Si (111) substrate [18]. A 2.5-μm-thick n-type $Al_{0.05}Ga_{0.95}N$ cladding layer is subsequently grown with a Si doping of 6×10^{18} cm^{-3}, followed by 108-nm-thick $In_{0.02}Ga_{0.98}N/Al_{0.10}Ga_{0.90}N$ superlattice layers, 105-nm-thick $InGaN/Al_{0.10}Ga_{0.90}N$ MQW structure, and a 80-nm-thick p-type $Al_{0.05}Ga_{0.95}N$ layer with a Mg doping of 3×10^{19} cm^{-3}. Finally, a 10-nm-thick Mg-doped GaN contact layer is deposited. Figure 1(b) shows a high-resolution TEM image of the five pairs of $InGaN/Al_{0.10}Ga_{0.90}N$ MQW active regions. The thicknesses of the low-In-content InGaN MQW layer and $Al_{0.10}Ga_{0.90}N$ barrier are 3 and 10 nm, respectively.

Figure 2 schematically illustrates the fabrication process flow of a monolithic NUV multicomponent system, its release from the silicon substrate, and its transfer and bonding to a foreign substrate [20]. Identical isolation mesas for the transmitter and receiver are defined by photolithography, and inductively coupled plasma reactive ion etching (ICP-RIE) is employed to expose the n-type AlGaN using Cl_2 and BCl_3 hybrid gases with flow rates of 10 and 25 sccm, respectively. Following electron beam evaporation and lift-off processes, both p- and n-contacts are obtained with 20/200 nm Ni/Ag metal stacks without thermal annealing procedure, leading to the formation of the MQW diodes. Both waveguide and support beams are defined and generated by ICP-RIE. The III-nitride-on-silicon platform substrate enables us to remove the silicon substrate using a wafer-level fabrication process flow. The top device structures are fully covered with thick photoresist for protection. Deep reactive ion etching is performed to etch the bottom silicon beneath the multicomponent system to obtain a suspended device architecture, and underside ICP-RIE is then carried out without an etching mask to decrease total thickness of the suspended membrane by etching away the common underlying slab to form a completely suspended support beam and waveguide. Mechanical release is conducted to directly transfer the suspended membrane from the host silicon substrate to a foreign substrate. Finally, the

transferred monolithic multicomponent system attached to the foreign substrate is wire-bonded to a test pad.

Figure 3(a) shows a scanning electron microscope (SEM) image of the monolithic multicomponent system on silicon. The whole multicomponent system, in which two MQW diodes with an identical MQW structure are produced by using the same process flow, is fabricated on a 0.8-mm-diameter suspended membrane. One MQW diode works as a transmitter to emit the modulated light and the other MQW diode functions as a receiver to detect the incident light. The transmitter interconnects with the receiver through a 6-μm-wide and 100-μm-long suspended waveguide. Figure 3(b) shows a magnified SEM image of the coupling butts. A three-dimensional atomic force microscope (AFM) image is illustrated in Figure 3(c). The generated mesa is approximately 453 nm in height and the gap between the n-electrode and mesa is about 7.6 μm. The support beams are mechanically fractured with probes, which directly release the 0.8-mm-diameter suspended membrane from the silicon to the foreign substrate. Figure 3(d) shows an optical image of the transferred monolithic multicomponent system on glass. The device transfer from the silicon substrate to the foreign substrate would also offer a novel approach to solve the serious heat dissipation aspect in opto-electronic devices to significantly increase device stability [26].

Figure 4(a) shows the measured current-voltage (I-V) curves of the transmitter on glass, exhibiting rectifying behavior with a turn-on voltage of 2.8 V. The transmitter and receiver can work independently because of the relatively high resistance between the two components. Figure 4(b) shows a light emission image of the two MQW-diodes. They are both biased at 4.5 V and function as emitters.

When the MQW diode functions as a transmitter, it emits light. The shift in wavelength

emission after device-structure transfer occurs because the built-in stress changes. In our case, we focused on the transferred MQW-diode [27-29]. The electroluminescence (EL) spectra of the transmitter-on-glass exhibit a dominant EL peak at 386 nm, as shown in Figure 5(a). Upon increasing the current injection of the transmitter from 1 to 3 mA, the EL emission intensity is increased. On the other hand, the MQW-diode can detect light when it acts as a receiver. The spectral responsivity of the receiver, which is measured through a combination of a micro-transmittance setup with a Horbia iHR320 spectrometer, is also illustrated in Figure 5(a). In the monolithic multicomponent system, the on-chip optical interconnect between the transmitter and receiver is realized through the suspended waveguide. A fraction of the light emitted from the transmitter is coupled to the suspended waveguide and finally, the receiver absorbs the guided light through suspended waveguide. Although the light emission of the transmitter may spread out to the free space, the on-chip optical interconnect is mainly realized through the waveguide because the transmitter and receiver lie in the same plane. There is a spectral overlap between the emission and responsivity spectra of the MQW diode [10, 22]. Since the transmitter and receiver have an identical MQW-diode architecture, the receiver can respond to the absorbed light, which corresponds to the emission spectra at shorter wavelengths of the transmitter. The number of photo-generated electron-hole pairs at the receiver is proportional to the current injection of the transmitter, which modulates the light emission intensity. Figure 5(b) shows the I-V characteristics and photocurrents of the receiver. At the receiver, the dark current is defined as the current when the current injection of the transmitter is zero. The photocurrents are thus normalized. With increasing current injection of the transmitter, the light emission becomes stronger and, thus, more light is absorbed by the receiver, leading to a larger photocurrent. The monolithically integrated receiver can sense the emission of the transmitter, resulting in the

multicomponent system with the capability of on-chip power monitoring in the NUV region.

Figure 6(a) shows a transferred chip on glass, which is wire-bonded to a test pad by West bond 7KE. The Ni/Ag electrode can function as a metal mirror to reflect the emitted light back to enhance the light output from the bottom interface. Figure 6(b) illustrates the light emission when the transmitter is biased at 4.5 V. The transferred transmitter is promising for free-space light communication.

Through a micro-transmittance setup [30], the wired-bonded transmitter on glass is directly driven by a Keysight 33600A arbitrary waveform generator. Using non-return-to-zero on-off keying modulation, the light emission is modulated with a peak-to-peak voltage V_{pp} of 3.5 V and an offset voltage V_{offset} of 2.2 V, and the pseudorandom binary sequence (PRBS 2^7-1) data streams are loaded. The spatial light emission is detected by a Hamamatsu C12702-11 photodiode module to generate the electrical signals, which are characterized by a digital storage oscilloscope. Figure 7(a) shows the transmitted and received PRBS data streams at a rate of 200 Mbps. The oscilloscope has an input impedance of 1MΩ and operates under AC coupling model. Figure 7(b) shows the measured eye diagrams at 200 Mbps. Error-free eyes are distinctly observed.

The III-nitride-on-silicon platform opens a new route to manufacturing and mechanically transferring the monolithic multicomponent systems with integrated functionalities. The two identical InGaN/$Al_{0.10}Ga_{0.90}N$ MQW diodes separately function as the transmitter and receiver, respectively, and the transmitter interconnects with the receiver using a suspended waveguide, leading to the formation of an on-chip optical interconnect. The receiver monitors the changes in emission of the transmitter due to the overlap of the emission and detection spectra of the MQW diodes. On the basis of on-off keying modulation, the wire-bonded transmitter-on-glass

experimentally demonstrates spatial NUV light transmission at 200 Mbps. Such a transferrable monolithic multicomponent system should contribute to the development of on-chip power monitors, free-space light communication and wearable optoelectronics in the NUV region.

Acknowledgements

This work was jointly supported by National Key R&D Program of China (2016YFE0118400), the Natural Science Foundation of Jiangsu Province (BE2016186), the National Natural Science Foundation of China (61531166004), and the “111” project.

References and Notes:

1. T.-N. Lin, S. R. M. Santiago, C.-T. Yuan, K.-P. Chiu, J.-L. Shen, T.-C. Wang, H.-C. Kuo, C.-H. Chiu, Y.-C. Yao, and Y.-J. Lee, "Enhanced Performance of GaN based Ultraviolet Light Emitting Diodes by Photon Recycling Using Graphene Quantum Dots," Sci. Rep. **7**, 7108 (2017).
2. K. H. Lee, Y.-T. Moon, J.-O. Song, and J. S. Kwak, "Light interaction in sapphire/MgF_2/Altriple-layer omnidirectional reflectors in AlGaN-based near ultraviolet light-emitting diodes," Sci. Rep. **5**, 9717 (2015).
3. Y.-K. Kuo, F.-M. Chen, J.-Y. Chang, and Y.-H. Shih, "Structural design and optimization of near-ultraviolet light-emitting diodes with wide wells," J. Appl. Phys. **9**, 77 (2016).
4. J. Sun, H. Q. Sun, X. Y. Yi, X. Yang, T.Y. Liu, X. Wang, X. Zhang, X. C. Fan, Z. D. Zhang, and Z. Y. Guo, "Efficiency enhancement in AlGaN deep ultraviolet light-emitting diodes by adjusting Mg doped staggered barriers," Superlattices Microstruct. **107**, 49-55 (2017).
5. K. Song, M. Mohseni, and F. Taghipour, "Application of ultraviolet light-emitting diodes (UV-LEDs) for water disinfection: A review," Water Res. **94**, 341-349 (2016).
6. Z. Y. Jiang, M. R. M. Atalla, G. J. You, L. Wang, X. Y. Li, J. Liu, A. M. Elahi, L. Wei, and J. Xu, "Monolithic integration of nitride light emitting diodes and photodetectors for bi-directional optical communication," Opt. Lett. **39**, 5657-5660 (2014).
7. Y. J. Wang, Y. Xu , Y. C. Yang , X. M. Gao, B. C. Zhu , W. Cai , J. L. Yuan, R. Zhang, and H. B. Zhu, "Simultaneous light emission and detection of InGaN/GaN multiple quantum well diodes for in-plane visible light communication on a chip," Opt. Commun. **387**, 440-445 (2017).
8. W. J. Zhang, L. Zhang, B. Wang, Z. M. Zhu, K. E. K. Lee, J. Michel, C. S.-J and L.-S Peh, "Ultralow-power LED-enabled on-chip optical communication designed in the III-Nitride and silicon CMOS process integrated platform," IEEE Des. Test. **31**, 36-45 (2014).
9. M. Marso, M. Mikulics, H. Lüth, Z. Sofer, P. Kordoš and H. Hardtdegen, "Hybrid optoelectronics based on a nanocrystal/III-N nano-LED platform," Advanced Semiconductor Devices and Microsystems (ASDAM) 77-80 (2016).
10. X. M. Gao, Z. Shi, Y. Jiang, C. Qin, and Y. J. Wang "Monolithic III-nitride photonic integration toward multifunctional devices," Opt. Lett. **42**, 4853-4856 (2017).
11. C. Shen, T. K. Ng, J. T. Leonard, A. Pourhashemi, H. M. Oubei, M. S. Alias, S. Nakamura, S. P. DenBaars, J. S. Speck, A. Y. Alyamani, M. M. Eldesouki, and B. S. Ooi, "High-

Modulation-Efficiency, integrated waveguide modulator-laser diode at 448 nm," ACS Photon. **3**, 262-268 (2016).

12. A. Dadgar, C. Hums, A. Diez, J. Bläsing, and A. Krost, "Growth of blue GaN LED structures on 150-mm Si(1 1 1)," J. Cryst. Growth **297**, 279–282 (2006).

13. K. Maki, T. Tanikawa, Y. Honda, and H. Amano, "Optically pumped lasing properties of (1101) InGaN/GaN stripe multiquantum wells with ridge cavity structure on patterned (001) Si substrates," Appl. Phys. Express **8**, 022702 (2015).

14. Y. Sun, K. Zhou, Q. Sun, J. P. Liu, M. X. Feng, Z. C. Li, Y. Zhou, L. Q. Zhang, D. Y. Li, S. M. Zhang, M. S. Ikeda, S. Liu and H. Yang, "Room-temperature continuous-wave electrically injected InGaN-based laser directly grown on Si," Nature Photon. **10**, 595-599 (2016).

15. C.-L. Tsai, Y.-C. Li, Y.-C. Lu, and S.-H. Chang, "Fabrication and characterization of Si substrate-free InGaN light-emitting diodes and their application in visible light communications," IEEE Photonics J. **9**, 8200612 (2017).

16. Y. Nanishi, "Nobel Prize in Physics: The birth of the blue LED," Nat. Photonics **8**, 884–886 (2014).

17. G. Q. Li, W. L. Wang, W. J. Yang, Y. H. Lin, H. Y. Wang, Z. T. Lin, and S. Z. Zhou, "GaN-based light-emitting diodes on various substrates: A critical review," Rep. Prog. Phys. **79**, 056501 (2016).

18. Z. C. Li, L. G. Liu, Y. N. Huang, Q. Sun, M. X. Feng, Y. Zhou, H. M. Zhao, and H. Zhao, "High-power AlGaN-based near-ultraviolet light-emitting diodes grown on Si(111)," Appl. Phys. Express **10**, 072101 (2017).

19. Z.-H. Zhang, C. S. Chu, C. H. Chiu, T. C. Lu, L. P. Li, Y. G. Zhang, K. K. Tian, M. Q. Fang, Q. Sun, H.-C. Kuo, and W. G. Bi, "UVA light-emitting diode grown on Si substrate with enhanced electron and hole injections," Opt. Lett. **42**, 4533-4536 (2017).

20. K. Chung, C.-H. Lee, and G.-C. Yi, "Transferable GaN layers grown on ZnO-coated graphene layers for optoelectronic devices," Science **330**, 655–657 (2010).

21. Y. Kobayashi, K. Kumakura, T. Akasaka, and T. Makimoto, "Layered boron nitride as a release layer for mechanical transfer of GaN-based devices," Nature **484**, 223–227 (2012).

22. Z. Shi, X. M. Gao, J. L. Yuan, S. Zhang, Y. Jiang, F. H. Zhang, Y. Jiang, H. B. Zhu, and Y. J. Wang, "Transferrable monolithic III-nitride photonic circuit for multifunctional optoelectronics", Appl. Phys. Lett. **111**, 241104 (2017).

23. C. Goßler, C. Bierbrauer, R. Moser, M. kunzer, K. Holc, W. Pletschen, K. Köhler, J. Wagner, M. Schwaerzle, P. Ruther, O. Paul, J. Neff, D. Keppeler, G. hoch, T. moser, and U. T. schwarz, "GaN-based micro-LED arrays on flexible substrates for optical cochlear implants," J. Phys. D: Appl. Phys. **47**, 205401 (2014).

24. Y. F. Cheung, K. H. Li, and H. W. Choi, "Flexible free-standing III-nitride thin films for emitters and displays," ACS Appl. Mater. Interfaces **8**, 21440–21445 (2016).

25. C.-H. Cheng, T.-W. Huang, C.-L. Wu, M. K. Chen, C. H. Chu, Y.-R. Wu, M.-H. Shih, C.-K. Lee, H.-C. Kuo, D.-P. Tsai, and G.-R. Lin,"Transferring the bendable substrateless GaN LED grown on thin C-rich SiC buffer layer to flexible dielectric and metallic plates," J. Mater. Chem. C **5**, 607-617 (2017).

26. M. Mikulics, P. Kordošc, A. Foxab, M. Kočand, H. Lüthab, Z. Sofere and H. Hardtdegen, "Efficient heat dissipation in AlGaN/GaN heterostructure grown on silver substrate," Appl. Mater. Today **7**, 134-137 (2017).

27. H. Hardtdegen, M. Hollfelder, R. Meyer, R. Carius, H. Münder, S. Frohnhoff, D. Szynka and H. Lüth, "MOVPE growth of GaAs using a N_2 carrier," J. Cryst. Growth 124, 420-426 (1992).

28. M. Mikulics, Y. C. Arango, A. Winden, R. Adam, A. Hardtdegen, D. Grützmacher, E. Plinski, D. Gregušová, J. Novák, P. Kordoš, A. Moonshiram, M. Marso, Z. Sofer, H. Lüth, and H. Hardtdegen, "Direct electro-optical pumping for hybrid CdSe nanocrystal/III-nitride based nano-light-emitting diodes," Appl. Phys. Lett. 108, 061107 (2016).

29. M. Mikulics and H. Hardtdegen, "Nano-LED array fabrication suitable for future single photon lithography," Nanotechnology 26, 185302 (2015).

30. M. S. Islim, R. X. Ferreira, X. Y. He, E. Y. Xie, S. Videv, S. Viola, S. Watson, N. Bamiedakis, R. V. Penty, I. H. White, A. E. Kelly, E. Gu, H. Haas and M. D. Dawson, "Towards 10 Gb/s orthogonal frequency division multiplexing-based visible light communication using a GaN violet micro-LED," Photonics Research **5**, A35-A43 (2017)

Figure Captions

Fig. 1. (a) Cross-sectional TEM image of III-nitride films on Si (111) substrate. (b) High-resolution TEM image of the InGaN/$Al_{0.10}Ga_{0.90}N$ MQW active region.

Fig. 2. Schematic illustration of the fabrication, release, transfer, and wire-bonding process flow for the monolithic NUV multicomponent system.

Fig. 3. (a) SEM image of the monolithic multicomponent system on silicon. (b) Magnified SEM image of the coupling butts consisting of the MQW-diode and suspended waveguide. (c) Three-dimensional AFM image of the coupling butts. (d) Optical image of the transferred monolithic multicomponent system.

Fig. 4. (a) Measured I-V curves of the transferred monolithic multicomponent system. (b) Light emission image of the two MQW diodes.

Fig. 5. (a) EL spectra and spectral responsivity of the InGaN/$Al_{0.10}Ga_{0.90}N$ MQW-diode. (b) Induced photocurrent at the receiver as a function of the current injection of the transmitter.

Fig. 6. (a) Wire-bonded multicomponent system on the glass substrate. (b) Light emission image of the wire-bonded multicomponent system at 4.5 V.

Fig. 7. (a) Transmitted and received PRBS data streams at 200 Mbps. (b) Eye diagrams for free-space light communication at a transmission rate of 200 Mbps.

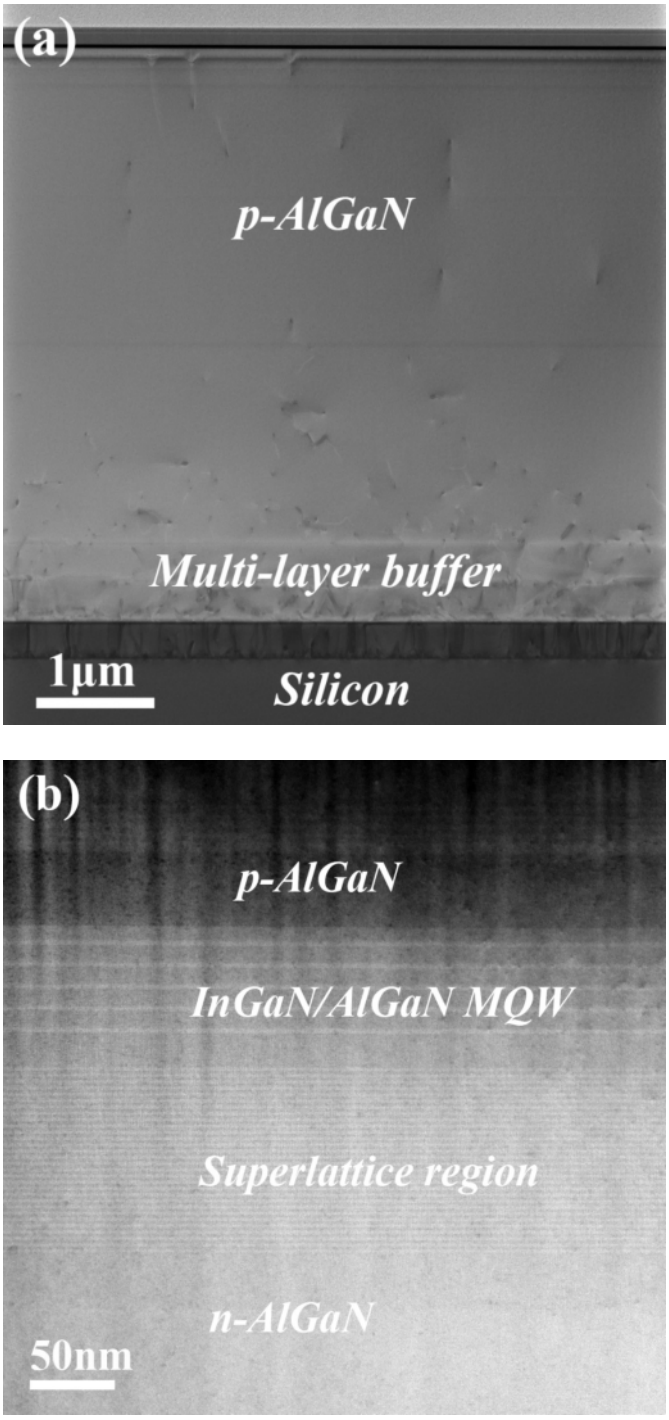

Figure 1

Chuan Qin et al.

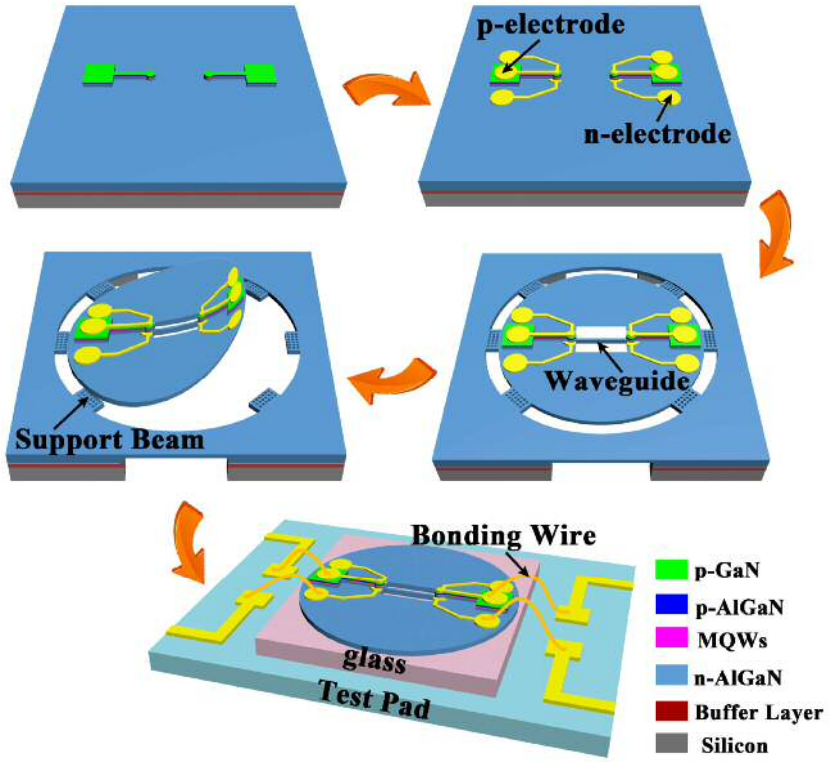

Figure 2

Chuan Qin et al.

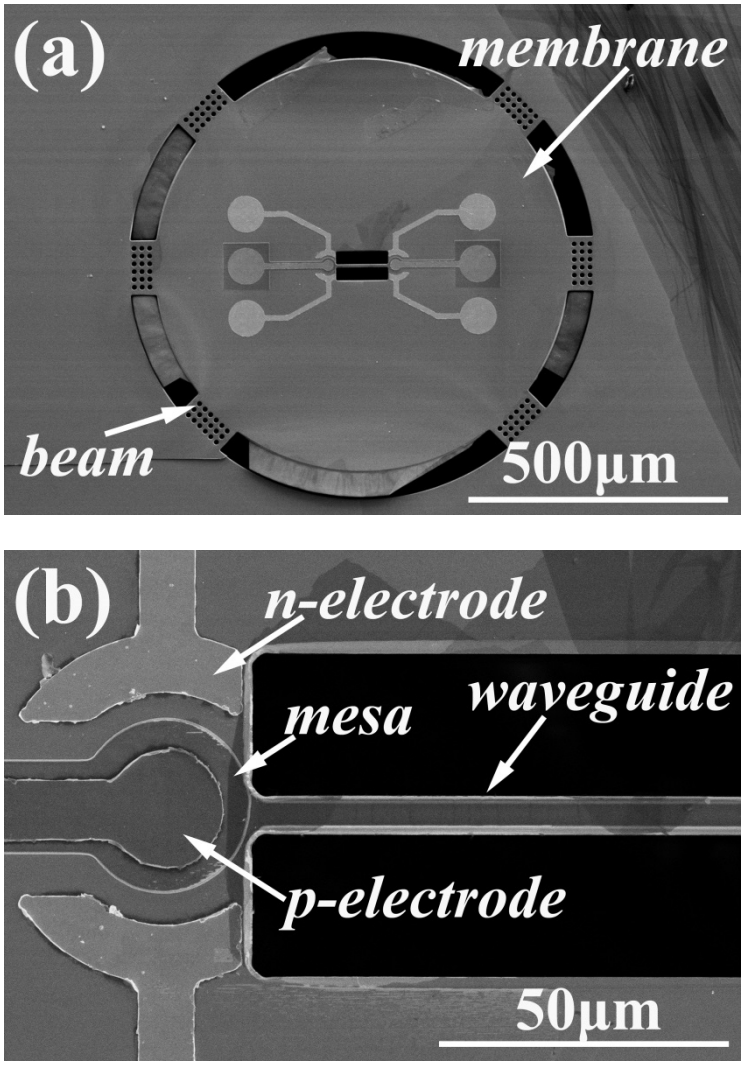
(a)
membrane
beam
500μm
(b)
n-electrode
mesa
waveguide
p-electrode
50μm

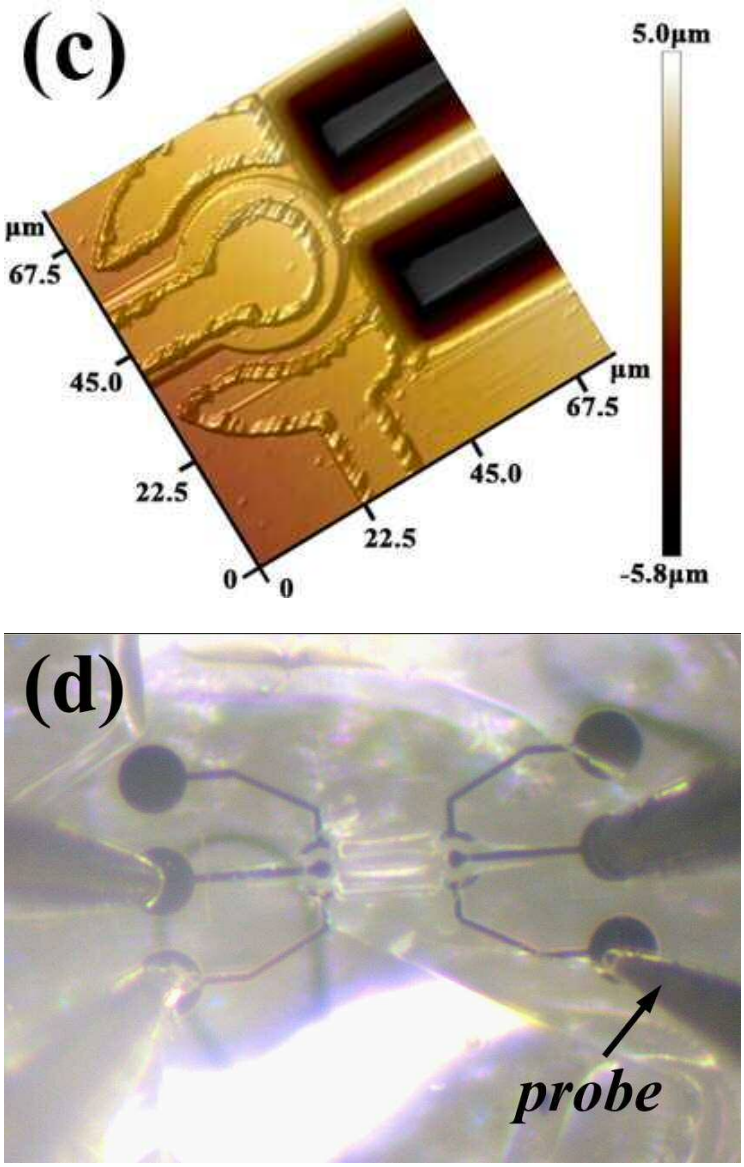

Figure 3

Chuan Qin et al.

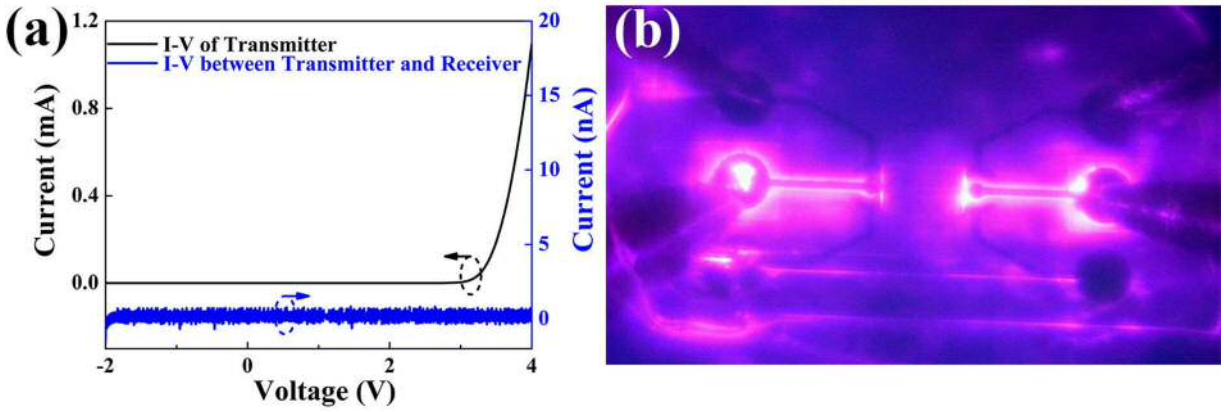

Figure 4

Chuan Qin et al.

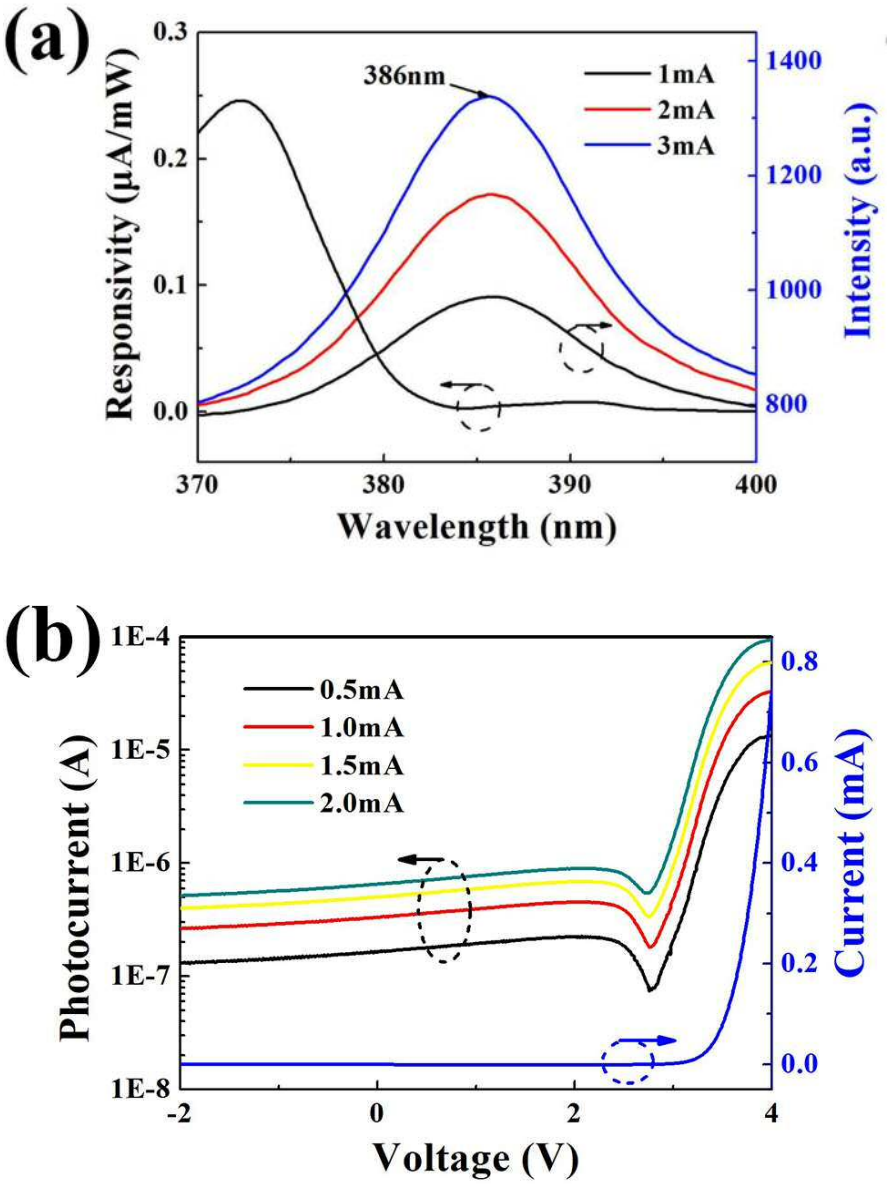

Figure 5

Chuan Qin et al.

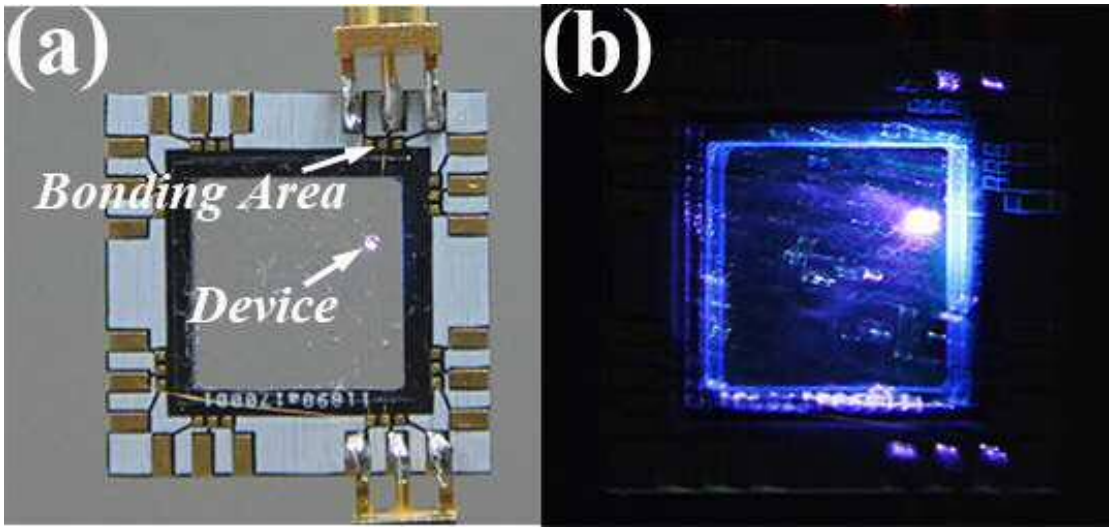

Figure 6

Chuan Qin et al.

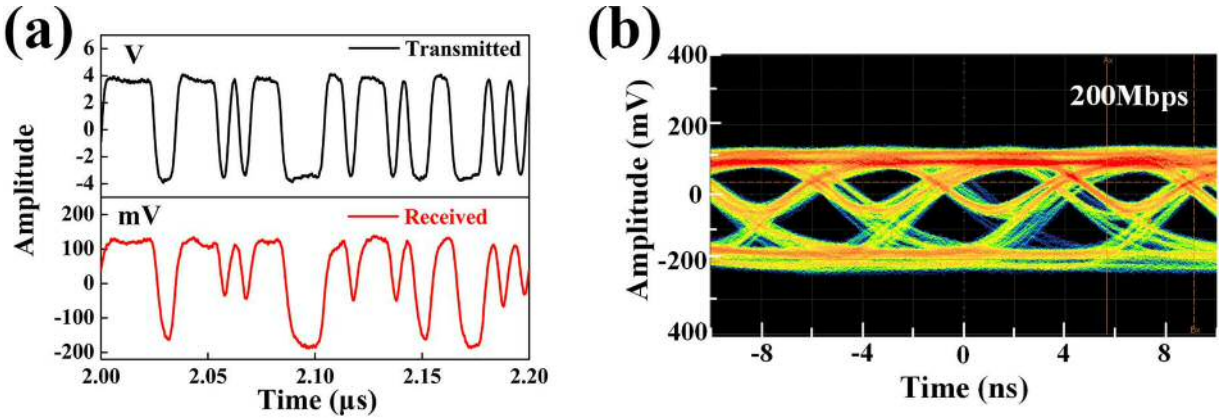

Figure 7

Chuan Qin et al.